THE JOURNAL OF PHYSICAL CHEMISTRY B

Article

pubs.acs.org/JPCB

Toward an Equation of State for Water inside Carbon Nanotubes

M. Sadeghi[†] and G. A. Parsafar*[,†,‡]

[†]Institute for Nanoscience and Nanotechnology (INST), Sharif University of Technology, Tehran, Iran

[‡]Department of Chemistry, Sharif University of Technology, Tehran, Iran

ABSTRACT: Water inside carbon nanotubes as an example of nanoconfined water has gained noticeable attention, in both theoretical and applied aspects. Molecular simulation has played a major role in the studies in this field. Yet, there is a need for systematic study of simulation results and compilation of scientifically reliable predictive relations. Here we present Monte Carlo simulations of water inside carbon nanotubes with different radii. An equation of state which was derived on the basis of the extended Lennard–Jones (12,6,3) as the effective pair potential is chosen for the system of water inside the carbon nanotubes. The equation of state is modified to take the effects of anisotropic pressure tensor into account. Using the simulation results, the applicability of this equation of state for water inside the carbon nanotubes is studied and the parameters of the equation of state for this system are obtained.

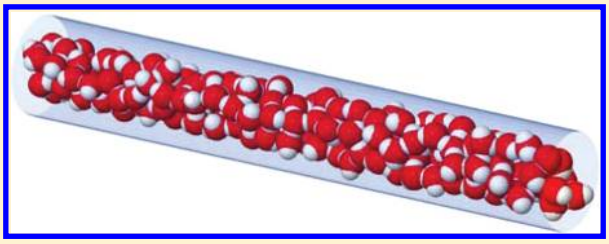

1. INTRODUCTION

The physical behavior of the so-called nanoconfined water has become of significant interest to researchers in recent years. Nanoconfined water is defined as the water trapped in nanosized geometries such as nanoslits, nanopores, and nanotubes. The behavior of nanoconfined water is of major importance in some specific areas of application, among which the ion-channels in biological systems,[1−4] lubrication of micro- and nanosized devices,[5,6] radioactive waste storage and heavy ion diffusion,[7−9] nanofluidic devices,[10−14] protein folding,[15−17] and water purification using nanotubes[18−21] are worth mentioning. Confinement of water in the nanosized spaces changes its physical and thermodynamic behavior drastically. Using X-ray diffraction (XRD) techniques, it has been shown that water confined inside carbon nanotubes (CNTs) retains its liquid state at temperatures far below its bulk freezing point.[22] When frozen, the nanoconfined water forms spectacular quasi-one-dimensional crystals known as ice nanotubes.[22,23] Using inelastic neutron scattering, it has also been observed that in nanoconfined water the hydrogen bond energy is reduced and the hydrogen bond network is weakened.[24,25] This leads to the softer dynamics of water molecules inside nanotubes.

Water has been the subject of computer simulation for more than three decades.[26] Simulation techniques have proven to be useful tools in studying the physical and thermodynamic behavior of water inside the nanotubes. In an early work, Lynden-Bell and Rasaiah used molecular dynamics to study the water confined in cylindrical nanopores with strictly repulsive walls.[27] They observed the formation of cylindrical water shells inside carbon nanotubes. Also, they studied the mobility of ions in this system and showed the different behavior of small and large ions. In 2001, Hummer et al. reported molecular dynamics simulations of water conduction through the hydrophobic channel of carbon nanotubes.[28] They observed instantaneous filling of carbon nanotubes with single-file chains of water molecules and pulse-like transmission of water through the CNTs. Striolo et al. conducted research in water adsorption in the nanopores using grand canonical Monte Carlo simulations.[29−32] By changing the chemical potential of the system, they obtained the adsorption−desorption isotherms for the nanotubes with different radii. They studied the effects of temperature, pore wall hydrophobicity, and connectivity of the pores on the water adsorption. In a more recent work, Lakatos and Patey also used the grand-canonical Monte Carlo simulation to study the adsorption of water in nanotubes.[33] They studied the effect of ions inside nanotubes on the adsorption behavior. Srivastava et al. used molecular dynamics to study the phase transition of water in graphite and mica slit pores.[34] They observed that the vapor−liquid coexistence occurs in different densities in the layers of the confined water. Gordillo and Marti used molecular dynamics in the canonical ensemble to study the hydrogen bonds of water inside carbon nanotubes.[35] Using conditions based on oxygen−hydrogen separation and alignment, they calculated the mean number of hydrogen bonds and showed that this number is smaller than its corresponding value in the bulk water. In another work, they also studied the hydrogen bonds of supercritical water inside the carbon nanotubes and showed the more prominent reduction in the number of hydrogen bonds.[36] Koga et al. used molecular dynamics simulation to study the freezing of water inside the carbon nanotubes and the formation of the ice nanotubes.[23] Their simulations predicted the formation of four different ice nanotubes with the square, pentagonal, hexagonal, and heptagonal cross sections, depending on the radius of the carbon nanotube. Using the simulation results, they studied the phase transition in the thermodynamic space of the nanotube

Received: December 4, 2011
Revised: March 23, 2012
Published: April 3, 2012

volume, temperature, and axial pressure. In a recent work, Kyakuno et al. conducted an extensive study on the global phase diagram of water confined inside carbon nanotubes.[37] They performed molecular dynamics simulations on the water confined inside CNTs with diameters ranging from 1.46 to 2.4 nm. Their results showed the wet−dry type transitions as well as the formation of ice nanotubes. They also used a combination of X-ray diffraction, nuclear magnetic resonance (NMR), and electrical resistance measurements to verify their simulation results.

Developing a general equation of state (EoS) for dense fluids and solids has been the major goal of much research.[38−46] Parsafar et al. employed an effective pair potential of the Lennard−Jones (12,6) type (originally named the averaged effective pair potential) to obtain an equation of state that mimics the linear isotherm regularity (LIR) in some dense fluids.[44,47] Parsafar and Mason used the repulsive branch of a universal expression for the binding energy of solids to obtain a simple cubic function for the potential energy in terms of density.[42] The accuracy of the EoS was further enhanced by considering an extended Lennard−Jones (12,6,3) interaction model as the effective pair potential, and it was shown that the new equation of state (EoS III) is applicable to a wide variety of fluids, including nonpolar, polar, hydrogen-bonded, and metallic, as well as all types of solids.[45]

In this paper, we first introduce a modified version of the EoS III originally developed by Parsafar et al.[45] As the pressure tensor for water inside the CNTs is anisotropic, two pressure components, axial and radial, are to be considered separately. Thus, we have modified the EoS III to include the axial and radial pressure components; hence, two separate equations of state, one for the axial and the other for the radial compressibility factors, are given. Using Monte Carlo simulations in canonical ensemble, we have calculated the thermodynamic parameters of water inside the CNTs with different radii. The anisotropic pressure tensor in this system has been calculated using the separated axial and radial virial expressions. Simulations have been performed for the nanotubes with different radii, both at the filled and unfilled states, with water. The parameters of the equations of state are calculated based on the simulation results, and it is shown that the EoS III is capable to model the water inside the CNTs with very good accuracy.

2. PRESSURE TENSOR AND THE THERMODYNAMIC EOS

For the water confined inside a nanotube, the radial and axial forces are different. Thus, water inside the nanotube is an anisotropic system for which the pressure tensor has to be used instead of a scalar pressure. The pressure in the axial and radial directions are denoted by p_L and p_R, respectively. The reversible work done by the water molecules in an expansion of cylindrical volume through the change in the radius, dR, and the change in the length, dL, is given by

$$\delta W_{rev} = (2\pi RL)p_R\, dR + (\pi R^2)p_L\, dL \tag{1}$$

Thus, at a constant number of particles, N, the Helmholtz free energy change is as follows:

$$dA = -SdT - (2\pi RL)p_R\, dR - (\pi R^2)p_L\, dL \tag{2}$$

At constant N and L, the Maxwell equation of eq 2 is

$$\left(\frac{\partial S}{\partial R}\right)_{N,L,T} = 2\pi RL\left(\frac{\partial p_R}{\partial T}\right)_{N,L,R} \tag{3}$$

Similarly, at constant N and R, the Maxwell equation of eq 2 is as follows:

$$\left(\frac{\partial S}{\partial L}\right)_{N,R,T} = \pi R^2\left(\frac{\partial p_L}{\partial T}\right)_{N,L,R} \tag{4}$$

From eq 2, the pressure components are given by

$$p_R = \frac{-1}{2\pi RL}\left(\frac{\partial A}{\partial R}\right)_{N,T,L} \tag{5a}$$

$$p_L = \frac{-1}{\pi R^2}\left(\frac{\partial A}{\partial L}\right)_{N,T,R} \tag{5b}$$

Because the Helmholtz free energy is defined as $A = U - TS$, at constant T and L,

$$\left(\frac{\partial A}{\partial R}\right)_{N,T,L} = \left(\frac{\partial U}{\partial R}\right)_{N,T,L} - T\left(\frac{\partial S}{\partial R}\right)_{N,T,L} \tag{6}$$

Substitution of $(\partial A/\partial R)_{N,T,L}$ from eq 5a and $(\partial S/\partial R)_{N,T,L}$ from eq 3 in eq 6 would result in

$$p_R = T\left(\frac{\partial p_R}{\partial T}\right)_{N,L,R} - \frac{1}{2\pi RL}\left(\frac{\partial U}{\partial R}\right)_{N,T,L} \tag{7}$$

Because $V = \pi R^2 L$ and $(\partial U/\partial R)_{N,T,L} = 2\pi RL(\partial U/\partial V)_{N,T,L}$, eq 7 may be rewritten as

$$p_R = T\left(\frac{\partial p_R}{\partial T}\right)_{N,L,R} - \left(\frac{\partial U}{\partial V}\right)_{N,T,L} \tag{8}$$

This is an exact thermodynamic EoS for the radial pressure. Similar manipulations would give the EoS for the axial pressure as

$$p_L = T\left(\frac{\partial p_L}{\partial T}\right)_{N,L,R} - \left(\frac{\partial U}{\partial V}\right)_{N,T,R} \tag{9}$$

Note that the internal energy, U, is the sum of kinetic energy of particles and the configurational potential energy,

$$U = N\left(u + \frac{6}{2}k_B T\right) \tag{10}$$

in which u is the configurational energy per particle, k_B is the Boltzmann constant, and $6/2k_BT$ is the mean kinetic energy of one water molecule with six translational and rotational degrees of freedom. Using eq 10, it is trivial to obtain $(\partial U/\partial v)_{N,T} = N(\partial u/\partial v)_{N,T} = (\partial u/\partial v)_{N,T}$ where $v = V/N$ is the molar volume. Thus, eqs 8 and 9 may be rewritten as

$$p_R = T\left(\frac{\partial p_R}{\partial T}\right)_{N,L,R} - \left(\frac{\partial u}{\partial v}\right)_{N,T,L} \tag{11a}$$

$$p_L = T\left(\frac{\partial p_L}{\partial T}\right)_{N,L,R} - \left(\frac{\partial u}{\partial v}\right)_{N,T,R} \tag{11b}$$

dx.doi.org/10.1021/jp211647e | J. Phys. Chem. B 2012, 116, 4943−4951

3. DENSITY DEPENDENCE OF CONFIGURATIONAL ENERGY

To use eqs 11a and 11b to find the radial and axial components of pressure tensor, it is necessary to know the density dependence of the configurational energy, u. The nature of intermolecular interactions, as well as the physical state of the system, determines how the configurational energy varies with density. For the system of water molecules inside the CNT, the extended Lennard−Jones model, first introduced by Parsafar et al., is used.[45] The extended Lennard−Jones model consists of two distinct parts, pertaining to short- and long-range interactions. The first part is a conventional (12,6) Lennard−Jones model that covers the short-range van der Waals interactions, which, in the case of the system under study, exists between water molecules as well as between water molecules and the carbon atoms of the CNT wall. But water molecules have permanent electric dipoles, and apart from van der Waals interactions, dipole−dipole electric interactions are also to be considered. Parsafar et al. extended the conventional (12,6) Lennard−Jones interaction by adding a $1/r^3$ term to account for long-range dipole−dipole interactions. In the case of bulk systems, on the basis of the effective near-neighbor pair interactions of an extended Lennard−Jones (12,6,3) type, Parsafar et al. showed that for a wide variety of fluids and solids, the average configurational energy per particle may be given by[45]

$$u = \frac{k_3(T)}{v} + \frac{k_6(T)}{v^2} + \frac{k_{12}(T)}{v^4} \tag{12}$$

The temperature-dependent parameters k_is depend on the chemical species as well as the physical state of the system. Equation 12 may be rearranged to

$$uv^2 = k_6(T) + \frac{k_3(T)}{\rho} + k_{12}(T)\rho^2 \tag{13}$$

where $\rho = 1/v$ is the molar density. The applicability of eq 13 to the system of water molecules inside the CNTs will be directly verified using the simulation results.

4. EQUATION OF STATE III FOR THE ANISOTROPIC SYSTEM

Following the notation used by Parsafar et al.[42,45] and using eq 11a, the exact thermodynamic EoS for the radial component of pressure tensor may be rewritten as

$$(Z_R - 1)v^2 = -\frac{1}{\rho^3 k_B T}\left(\frac{\partial u}{\partial v}\right)_{N,T,L} + a_{2,R} \tag{14}$$

where $Z_R = p_R v/k_B T$ is the radial compressibility factor and

$$a_{2,R}(T) = \frac{1}{\rho^2}\left[\frac{1}{\rho k_B}\left(\frac{\partial p_R}{\partial T}\right)_{N,L,R} - 1\right] \tag{15}$$

is the contribution from the nonideal thermal pressure. Substituting the configurational energy per particle from eq 12, the equation of state 14 is rewritten as

$$\begin{aligned}(Z_R - 1)v^2 &= \frac{1}{k_B T}\left[2k_6(T) + \frac{k_3(T)}{\rho} + 4k_{12}(T)\rho^2\right] + a_{2,R}(T) \\ &= F_{6,R}(T) + \frac{F_{3,R}(T)}{\rho} + F_{12,R}(T)\rho^2 + a_{2,R}(T)\end{aligned} \tag{16}$$

A similar equation is obtained for the axial compressibility factor, Z_L, as

$$(Z_L - 1)v^2 = F_{6,L}(T) + \frac{F_{3,L}(T)}{\rho} + F_{12,L}(T)\rho^2 + a_{2,L}(T) \tag{17}$$

in which

$$Z_L = p_L v/k_B T$$

$$a_{2,L}(T) = \frac{1}{\rho^2}\left[\frac{1}{\rho k_B}\left(\frac{\partial p_L}{\partial T}\right)_{N,L,R} - 1\right] \tag{18}$$

Equations 16 and 17 give the EoS III (as is named by Parsafar et al.[45]) in the radial and axial directions for the anisotropic system of water inside a nanotube, respectively. These equations of state can be expressed as follows

$$(Z_L - 1)v^2 = f_L + \frac{g_L}{\rho} + h_L\rho^2 \tag{19a}$$

$$(Z_R - 1)v^2 = f_R + \frac{g_R}{\rho} + h_R\rho^2 \tag{19b}$$

where $f_L = F_{6,L}(T) + a_{2,L}(T)$, $f_R = F_{6,R}(T) + a_{2,R}(T)$, $g_L = F_{3,L}(T)$, $g_R = F_{3,R}(T)$, $h_L = F_{12,L}(T)$, and $h_R = F_{12,R}(T)$. The parameters f, g, and h are nontrivial functions of temperature and in general contain contributions from both the internal and thermal pressures.

5. FILLED AND UNFILLED STATES

As will be shown on the basis of the simulation results, two distinct regimes are observed in the thermodynamic behavior of water confined in the CNTs. These two regimes correspond to the filled and unfilled states and are differentiated based on the density of water inside the CNTs. In the unfilled state, the water molecules do not completely fill the cylindrical space inside the CNT. Thus, the average distance among the nearest neighbor of water molecules is larger than that of the bulk water at the same temperature. Water molecules in this state form separate clusters in the available volume inside the CNT. In the unfilled state, the increase in the number of molecules increases the effective density but does not change the packing of water molecules. But in the filled state, the volume available to water molecules is completely filled and the addition of extra molecules leads to an extra packing. Thus, the density dependence of the configurational energy as well as radial and axial pressure components are expected to be different in these two states.

The density of water inside the CNT should be calculated based on the accessible volume corresponding to the effective radius of the CNT. The definition of the effective radius of the CNT is somewhat ad hoc. Here a definition based on the

dx.doi.org/10.1021/jp211647e | J. Phys. Chem. B 2012, 116, 4943−4951

interaction potential which will be given in eq 20 is used. The effective radius of a CNT is defined as the radial coordinate which corresponds to one k_BT of the water−wall interaction potential. With this definition, the effective radii of 0.16, 0.26, 0.36, and 0.46 nm are obtained for the CNTs with the geometric radii of 0.44, 0.54, 0.64, and 0.74 nm, respectively.

Considering the van der Waals radius of water molecules to be $1/2\sigma_{wt-wt}$, a value of 0.16 nm is obtained for this parameter (see Table 1). It is seen that the 0.44 nm CNT with the effective radius of 0.16 nm is filled with only a single array of water molecules. Thus, it is the smallest CNT appropriate for this study. Complete filling of the 0.44 nm CNT results in the average number density of 3.16 water molecules per nanometer length of the filled CNT, which corresponds to the molar density of 67.75 mol/L. It will be shown, based on the simulation results, that the transition from the unfilled state to filled state begins at the molar density of about 75 mol/L. For the CNTs with larger radii, calculating the filling density is not straightforward, but it is expected that the filling density be different for each CNT, especially when the radius of the CNT is comparable to the van der Waals radius of the water molecules.

Table 1. Parameters of the Water−Water and Water−Wall Potential Models

Water−Water (SPC/E)					
σ_{wt-wt} (nm)	ε_{wt-wt} (kJ/mol)	q_O (e)	q_H (e)	r_{OH} (nm)	∠HOH (deg)
0.3169	0.6502	−0.8476	0.4238	0.1	109.47
Water−Wall (L−J)					
σ_{wt-wl} (nm)	ε_{wt-wt}(kJ/mol)				
0.3283	0.3891				

6. SIMULATION DETAILS

Simulations are carried out using the Monte Carlo method in the canonical ensemble. The simulation box consists of water molecules placed inside a cylindrical volume representing a carbon nanotube. The water−water interaction energy is modeled using the well-established simple point charge/extended (SPC/E) potential. The SPC/E potential employs a three-point charge model of the water molecule with the Columbic interactions among the concentrated charges on the atoms of two molecules (q_O on the oxygen and q_H on the hydrogen atoms). Also, a van der Waals interaction with parameters σ_{wt-wt} and $\varepsilon_{wt-wt}$is considered between the oxygen atoms of two water molecules. The parameters of the SPC/E potential as well as the geometry of the water molecule used in this model are given in Table 1.[27,33,48]

The interaction of water molecules with the CNT wall is modeled using the (12,6) Lennard−Jones potential model. The CNT wall is considered to be electrically neutral, and no Columbic interactions exist between the molecules and the CNT wall. The CNT wall is considered as an infinitely long cylinder consisting of uniformly distributed van der Waals interaction sites with the surface density of n. Integrating the (12,6) Lennard−Jones potential on a smooth cylinder with an infinite length yields the following potential function inside the cylinder[49]

$$U_{wall}(r) = (n\pi^2)(\varepsilon_{wt\text{-}wl}\sigma_{wt\text{-}wl}^2)\left[\frac{63}{32}F\left(-\frac{9}{2}, -\frac{9}{2}; 1; \left(\frac{r}{R}\right)^2\right)\left(\left(\frac{R-r}{\sigma_{wt\text{-}wl}}\right)\left(1+\frac{r}{R}\right)\right)^{-10} - 3F\left(-\frac{3}{2}, -\frac{3}{2}; 1; \left(\frac{r}{R}\right)^2\right)\left(\left(\frac{R-r}{\sigma_{wt\text{-}wl}}\right)\left(1+\frac{r}{R}\right)\right)^{-4}\right] \quad (20)$$

in which σ_{wt-wl} and ε_{wt-wl} are the parameters of the Lennard−Jones potential, r is the radial coordinate of particles inside the cylinder, R is the radius of the cylinder, and F denotes the standard hypergeometric function. The water−wall interaction site on water molecules is set on the oxygen atoms. The parameters of the water−wall Lennard−Jones potential, which are given in Table 1, are calculated using the Lorentz−Berthelot mixing rule.[50] The surface density of interaction sites on the CNT wall is taken to be n = 40 nm^{-2}.[33]

As the water molecules are trapped inside the nanotube, the periodic boundary conditions are applied only in the axial direction of the CNT. The minimum image convention is used to model the periodic boundary conditions in the simulation box.[50,51] Note that the minimum image convention does not affect the water−wall interaction potential, because it is obtained by using the integration on an infinite cylinder. But water−water interactions are truncated for the distances larger than the half of the simulation box length. The length of the cubic simulation box is taken to be 4.0 nm, which corresponds to a cutoff radius of 2.0 nm for water−water interactions. This cutoff radius has been previously used for simulations of water inside the CNTs and has successfully reproduced observed behaviors in this system.[37,52]

Monte Carlo simulation in the canonical ensemble is performed using the Metropolis algorithm.[53] Independent trial moves for the translation and rotation of water molecules are used. Rigid-body rotations of water molecules are implemented by using unit-norm quaternions. This is a necessity to satisfy the symmetry requirements of the underlying Markov chain.[51] The magnitudes of the translational and rotational moves are chosen so that the acceptance rate for both translations and rotations fall in the vicinity of 50%. Simulation of systems with different water densities is achieved through changing the number of water molecules inside the section of CNT which is bounded in the simulation box.

Simulations are carried out at the constant temperature of 298 K. In all simulations, the system is brought to equilibrium in 10^7 steps before any data extraction. A minimum number of necessary steps for equilibration is chosen by monitoring the change of the total potential energy of the system versus the number of steps. In about 10^7 steps, the variations of potential energy are reduced to the random fluctuations about its mean value. After reaching equilibrium, 3×10^7 steps are simulated for the data collection. In evenly distributed sampling steps, the water−water and water−wall interaction energies as well as the axial and radial components of pressure are calculated. To calculate the pressure components, the following virial expressions are used:[27,33]

$$p_R = \frac{1}{2V}\left[2Nk_BT + \left\langle \sum_i \sum_{j>i} f_{ij}^x x_{ij} \right\rangle + \left\langle \sum_i \sum_{j>i} f_{ij}^y y_{ij} \right\rangle + \left\langle \sum_i \sum_{j>i} f_i^{wall}(R - r_i) \right\rangle\right] \quad (21a)$$

$$p_L = \frac{1}{V}\left[(N-2)k_BT + \left\langle \sum_i \sum_{j>i} f_{ij}^z z_{ij} \right\rangle\right] \quad (21b)$$

where f_{ij}^x, f_{ij}^y, and f_{ij}^z are the components of intermolecular forces between the ith and the jth water molecules in the x, y, and z directions, respectively, and f_i^{wall} is the force exerted by the ith molecule on the CNT wall. The coordinates x_{ij}, y_{ij}, and z_{ij} are the components of the intermolecular separation, and r_i is the radial coordinate of the ith molecule.

To produce more reliable results, in each specific simulation case, a total of eight separate simulations are carried out in parallel and the results are averaged out. As each simulation starts with a random arrangement of water molecules and hence a different point in the configurational phase space, using parallel simulations increases the overall coverage of the phase space.

7. RESULTS AND DISCUSSION

Before any discussions on the EoS, it is necessary to show the difference of filled and unfilled states of water inside the CNTs. The difference between the filled and unfilled states is best recognized by studying the behavior of the radial and axial pressure components. The Monte Carlo simulations are performed on water inside four different CNTs with radii of 0.44, 0.54, 0.64, and 0.74 nm, respectively. For each CNT, several simulations with a different number of water molecules are performed. All simulations are carried out in the *NVT* ensemble with the constant temperature of 298 K. The density of water is calculated using the definition of effective radius presented in the simulation details. The radial and axial pressures are calculated using eqs 21a and 21b. Figures 1 and 2 show the results of these simulations as the mean radial pressure (p_R) and mean axial pressure (p_L) versus the molar density of water (ρ) inside the CNTs. These figures show that the pressures follow two distinct regimes. In the case of each CNT, the density dependence of pressures changes at a certain density, which corresponds to the filling of the CNT with water molecules. For densities below the filling density, the pressure–density diagram is more or less linear. This behavior is a reminder of the ideal gas with zero interactions between the gas particles. In the case of water molecules inside the CNTs in the unfilled state, water clusters behave as separate particles with negligible interactions between the clusters. For densities above the filling density, the water clusters are merged and the pressure–density behavior deviates from the linear relation as the intermolecular interactions become important. Before the merging of the water clusters, the increase in density reduces the separation of the water clusters. As the water clusters move closer, the attractive interactions among the clusters cause a sudden drop in the pressures before the filling occurs. The filling densities are obtained as 75.14, 74.25, 62.39, and 55.82 mol/L for the 0.44, 0.54, 0.64, and 0.74 nm CNTs, respectively. With the increase of the CNT radius, the filling density converges to the molar density of the bulk water at 298 K which is 55.5 mol/L.

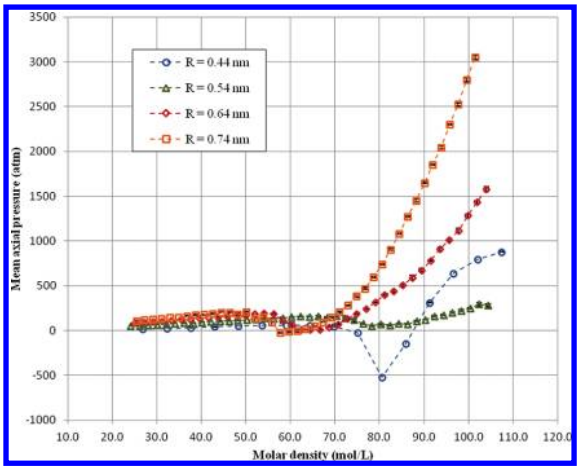

Figure 1. Mean axial pressure versus water density inside the CNTs with the given radii at T = 298 K (the dash lines are shown to guide the eye).

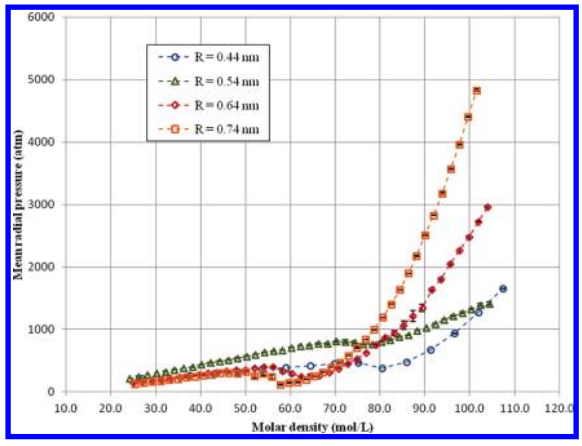

Figure 2. Mean radial pressure versus water density inside the CNTs with the given radii at T = 298 K (the dash lines are shown to guide the eye).

To show the transition between the unfilled and filled regimes more clearly, the Helmholtz free energy of water as a function of density is also calculated from the simulations. The free energy has been calculated using the particle addition technique.[50] Figure 3 shows the molar Helmholtz free energy for water inside the CNTs with a radii of 0.44, 0.54, 0.64, and 0.74 nm. A change of slope occurs in the free energy diagram versus density at the unfilled–filled transition. The dependency of the filling density on the radius of the CNT is easily observed in Figure 3, changing from 55.8 mol/L for R = 0.74 nm to 75.1 mol/L for R = 0.44 nm, respectively. Figure 4 shows the density profiles of water inside the four CNTs in the axial direction (along the length of the CNTs). For each CNT, density profiles are depicted for two different densities, namely below and above the filling density. In the unfilled state, the density profile of separate water clusters are distinguished, whereas in the filled state, approximate smooth density distribution can be seen. Note that in case of the 0.44 nm CNT, only a single array of water molecules is present inside the CNT and that gives rise to the oscillating density profiles (see Figure 4a).

In obtaining the equations of state 19a and 19b, it was assumed that the configurational energy of the fluid is

dx.doi.org/10.1021/jp211647e | J. Phys. Chem. B 2012, 116, 4943–4951

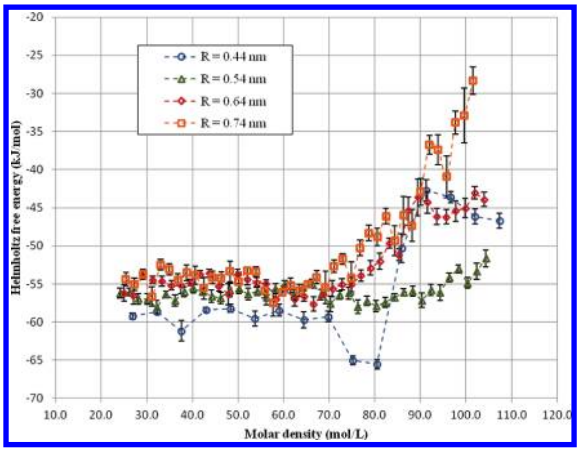

Figure 3. Helmholtz free energy per mole of water inside the CNTs with the given radii at T = 298 K (the dash lines are shown to guide the eye).

calculated using the extended Lennard–Jones interactions and is given by eq 12.[45] To verify the validity of this assumption for water inside the CNTs, the density dependence of the configurational energy is to be studied. For this purpose, the mean value of the quantity uv^2 is calculated, based on the Monte Carlo results, and its behavior is compared with the relation given in eq 13. As was shown for the pressures, the system of water inside the CNTs follows two distinct regimes in the filled and unfilled states. Thus, the density dependence of the configurational energy is studied for these two states, separately. Figures 5 and 6 show the uv^2 versus the molar density of water inside the four CNTs with radii of 0.44, 0.54, 0.64, and 0.74 nm for both the filled and unfilled states,

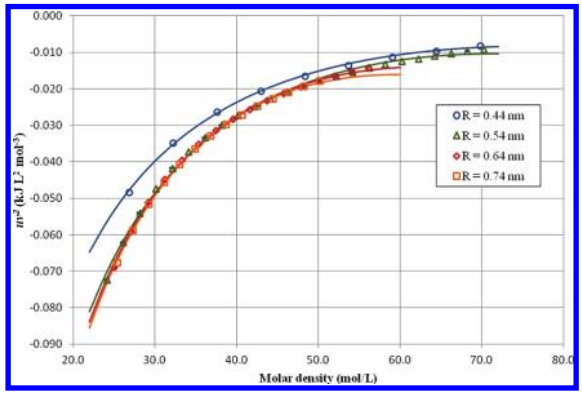

Figure 5. Density dependence of the configurational energy for the unfilled state of water inside the CNTs with the given radii at T = 298 K. Equation 13 is well fitted onto the simulation results for all CNTs.

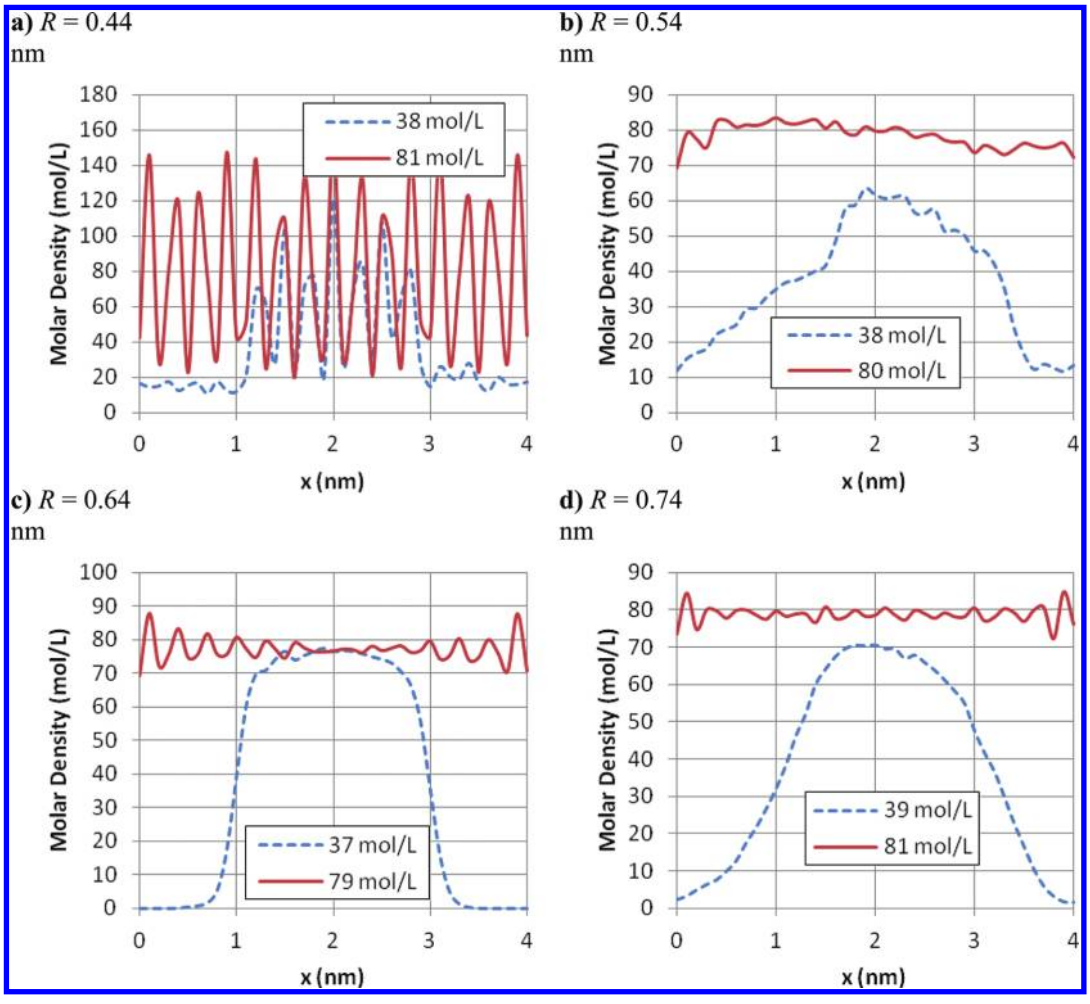

Figure 4. Density profiles of water inside the CNTs for the unfilled and filled states, with a CNT radius of (a) 0.44 nm, (b) 0.54 nm, (c) 0.64 nm, and (d) 0.74 nm.

dx.doi.org/10.1021/jp211647e | J. Phys. Chem. B 2012, 116, 4943–4951

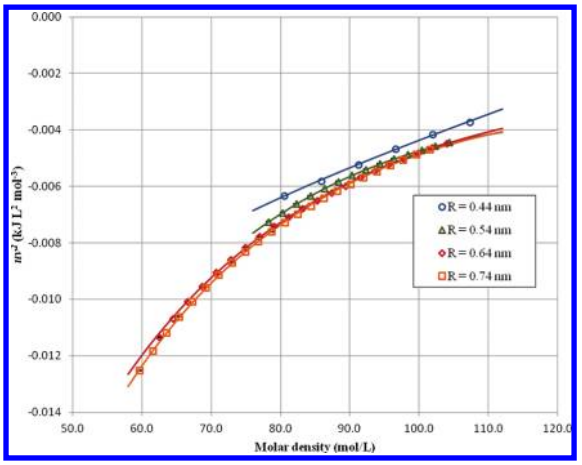

Figure 6. Density dependence of the configurational energy for the filled state of water inside the CNTs with the given radii at $T = 298$ K. Equation 13 is well fitted onto the simulation results for all CNTs

respectively. Solid lines are fitted curves based on the relation given in eq 13. The parameters of the fitted curves and the R^2 values of the least-squares method used for the regression are given in Table 2. In general, the R^2 values in both states show

Table 2. Parameters of the Fit to the Configuration Energy Relation Eq 13

radius (nm)	k_3 (kJ L mol^{-2})	10^2k_6 (kJ L^2 mol^{-3})	10^6k_{12} (kJ L^4 mol^{-5})	R^2
		Unfilled State		
0.44	−2.137	3.349	−2.360	0.9991
0.54	−2.815	4.876	−3.860	0.9981
0.64	−3.096	5.992	−6.220	0.9992
0.74	−3.251	6.610	−7.760	0.9996
		Filled State		
0.44	−0.478	−0.192	0.233	0.9990
0.54	−1.314	1.132	−0.292	1.0000
0.64	−1.254	0.960	−0.188	0.9998
0.74	−1.376	1.153	−0.264	0.9998

very good correlation between the simulations results and the predicted relation for the configurational energy. This verifies the applicability of the assumption of the (12,6,3) extended Lennard−Jones interactions. A more specific discussion concerning the effect of the CNT radius on the density dependence of the configurational energy may be presented. Figures 5 and 6 show that the density dependence of the configurational energy for water inside the 0.44 nm CNT is different from that for water inside the larger CNTs, to some extent. Also, unlike water inside the 0.44 nm CNT, uv^2 for water inside the CNTs with radii of 0.54, 0.64, and 0.74 nm converges to the same value at large densities. This can be related to the fact that inside a 0.44 nm CNT, water molecules are arranged in a single-file fashion, due to the small radius. Thus, the water−water interactions are restricted to the axial direction, allowing the water−wall interactions to prevail, especially for small molar densities.

To study the applicability of the EoS III given by eqs 19a and 19b for water inside the CNTs, the radial and axial compressibility factors are to be calculated. The mean values of $(Z_L - 1)v^2$ and $(Z_R - 1)v^2$ for the four CNTs in the unfilled state are shown versus the molar density in Figures 7 and 8. The parameters of the fit to the EoS III are given in Table 3. In

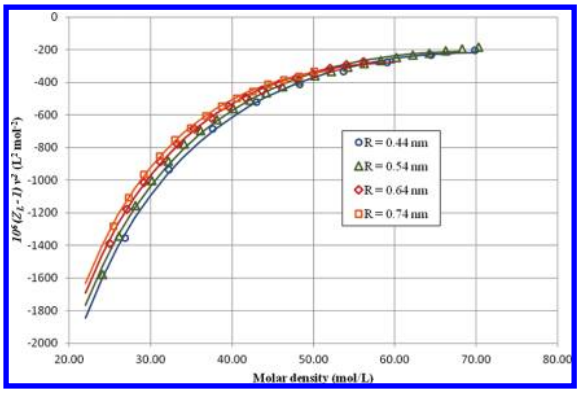

Figure 7. Fits of eq 19a onto the calculated data of the unfilled state, for the CNTs with the given radii.

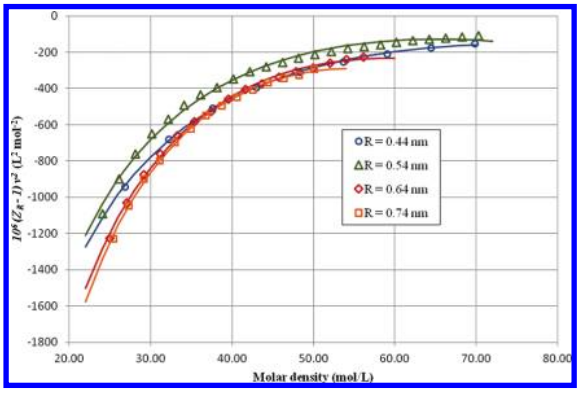

Figure 8. Fits of eq 19b onto the calculated data of the unfilled state, for the CNTs with the given radii.

the unfilled state, water inside four different CNTs follows the EoS III quite accurately.

For the filled state, the applicability of the EoS III is studied by plotting the mean values of $(Z_L - 1)v^2$ and $(Z_R - 1)v^2$ versus the molar density, as shown in Figures 9 and 10. The parameters of these fits, which are also given in Table 3, are

Table 3. Parameters of the Fit to the Axial and Radial Equations of State 19a and 19b

radius (nm)		f (L^2/mol^2)	$10^{-4}g$ (L/mol)	10^2h (L^3/mol^3)	R^2
		Unfilled State			
0.44	$10^6(Z_L - 1)v^2$	1161	−6.510	−9.140	0.9981
	$10^6(Z_R - 1)v^2$	689.7	−4.270	−4.850	0.9995
0.54	$10^6(Z_L - 1)v^2$	1173	−6.360	−9.720	0.9973
	$10^6(Z_R - 1)v^2$	935.6	−4.630	−8.320	0.9948
0.64	$10^6(Z_L - 1)v^2$	1305	−6.440	−14.10	0.999
	$10^6(Z_R - 1)v^2$	1279	−5.970	−14.40	0.9987
0.74	$10^6(Z_L - 1)v^2$	1393	−6.470	−17.70	0.9995
	$10^6(Z_R - 1)v^2$	1510	−6.580	−20.00	0.9991
		Filled State			
0.44	$10^6(Z_L - 1)v^2$	1674	−12.50	−4.960	0.9992
	$10^6(Z_R - 1)v^2$	115.3	−2.200	0.502	0.9995
0.54	$10^6(Z_L - 1)v^2$	239.2	−2.960	−0.337	0.9994
	$10^6(Z_R - 1)v^2$	244.5	−2.480	−0.427	0.9989
0.64	$10^6(Z_L - 1)v^2$	411.0	−4.060	−0.520	0.9995
	$10^6(Z_R - 1)v^2$	317.2	−3.440	0.289	0.9991
0.74	$10^6(Z_L - 1)v^2$	354.5	−3.950	0.608	0.9991
	$10^6(Z_R - 1)v^2$	190.5	−3.100	2.06	0.9996

dx.doi.org/10.1021/jp211647e | J. Phys. Chem. B 2012, 116, 4943−4951

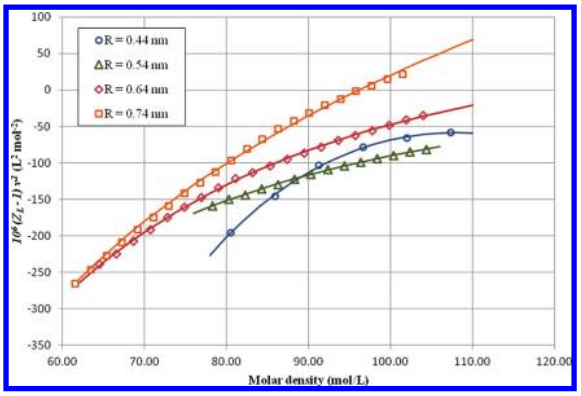

Figure 9. Fits of eq 19a onto the calculated data of the filled state, for the CNTs with the given radii.

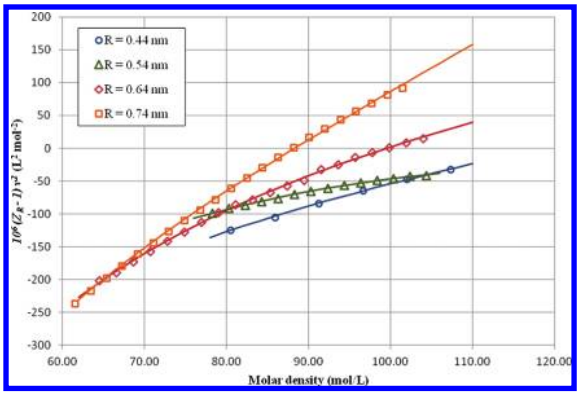

Figure 10. Fits of eq 19b onto the calculated data of the filled state, for the CNTs with the given radii.

drastically different from those of the unfilled state. On the basis of the R^2 values of the fits given in Table 3, the EoS III gives very accurate predictions for the filled state for all the CNTs as well.

In the unfilled state, the radial and axial compressibility factors of water inside the 0.44, 0.54, 0.64, and 0.74 nm CNTs have small dependency on the CNT radius. But in the filled state, the radius of the CNT has significant effect on the density dependence of the compressibility factor and the parameters of the equations of state in both radial and axial directions. Also the compressibility factor of water inside the 0.54 nm CNT has a significantly different behavior in the filled state. This behavior can be related to the arrangement and ordering of water molecules inside this CNT. Water molecules inside the 0.54 nm CNT are not in the single-file arrangement as in the case for 0.44 nm CNT, but considering that the effective diameter of this CNT is about 1.6 times the van der Waals diameter of the water molecules, it is reasonable to believe that water molecules are still strongly restricted in the radial direction. A more detailed discussion of this case, which is beyond the scope of this paper, is necessary and will be addressed in future works.

8. CONCLUSION

We have presented a Monte Carlo study of water inside the CNTs in the canonical ensemble and examined the predictive power of the EoS III. By considering the anisotropic pressure tensor for the water inside the CNTs, two separate equations of state for the radial and axial directions have been derived. The assumption of the nearest-neighbor extended Lennard–Jones interactions has been used in the derivation of the equations of state. Monte Carlo simulations are performed using a simulation box consisting of water molecules inside the cylindrical CNTs with the periodic boundary conditions in the axial direction. The water–water and water–wall interactions are modeled using the SPC/E and Lennard–Jones potentials, respectively. The simulation results have shown the difference in thermodynamic behavior of water inside the CNTs in the filled and unfilled states. Calculation of the interaction energies obtained from the Monte Carlo simulations has verified the applicability of the extended Lennard–Jones potential model for this system. Using the simulation results, the compressibility factors in both radial and axial directions in the unfilled and filled states have been calculated. The EoS III in the radial and axial directions has been fitted to these results with very good accuracies. The effect of radius and the filling of the CNTs on the configurational energy and the parameters of the equations of state have been discussed.

AUTHOR INFORMATION

Corresponding Author

*Phone: (+9821) 66165355. Fax: (+9821) 66005718, 66012983. E-mail: MohsenSadeghi@mehr.sharif.edu.

Notes

The authors declare no competing financial interest.

ACKNOWLEDGMENTS

The authors acknowledge financial support from the Sharif University of Technology research council. Also, the authors are grateful to G. Lakatos and G. N. Patey of the University of British Columbia for their useful comments regarding the Monte Carlo simulations.

REFERENCES

(1) Beckstein, O.; Biggin, P. C.; Bond, P.; Bright, J. N.; Domene, C.; Grottesi, A.; Holyoake, J.; Sansom, M. S. P. *FEBS Lett.* **2003**, *555*, 85–90.
(2) Beckstein, O.; Biggin, P. C.; Sansom, M. S. P. *J. Phys. Chem. B* **2001**, *105*, 12902–12905.
(3) Beckstein, O.; Sansom, M. S. P. *Phys. Biol.* **2004**, *1*, 42–52.
(4) Tieleman, D. P.; Biggin, P. C.; Smith, G. R.; Sansom, M. S. P. *Q. Rev. Biophys.* **2001**, *34*, 473–561.
(5) Scherge, M.; Li, X.; Schaefer, J. A. *Tribol. Lett.* **1999**, *6*, 215–220.
(6) Sirghi, L. *Appl. Phys. Lett.* **2003**, *82*, 3755–3757.
(7) Malikova, N.; Cadene, A.; Marry, V.; Dubois, E.; Turq, P. *J. Phys. Chem. B* **2006**, *110*, 3206–3214.
(8) Malikova, N.; Cadene, A.; Marry, V.; Dubois, E.; Turq, P.; Zanotti, J. M.; Longeville, S. *Chem. Phys.* **2005**, *317*, 226–235.
(9) Rotenberg, B.; Marry, V.; Dufreche, J. F.; Malikova, N.; Giffaut, E.; Turq, P. *C. R. Chim.* **2007**, *10*, 1108–1116.
(10) Daiguji, H. *Chem. Soc. Rev.* **2010**, *39*, 901–911.
(11) Daiguji, H.; Adachi, T.; Tatsumi, N. *Phys. Rev. E* **2008**, *78*, 026301.
(12) Daiguji, H.; Yang, P. D.; Majumdar, A. *Nano Lett.* **2004**, *4*, 137–142.
(13) Karlsson, A.; Karlsson, M.; Karlsson, R.; Sott, K.; Lundqvist, A.; Tokarz, M.; Orwar, O. *Anal. Chem.* **2003**, *75*, 2529–2537.
(14) Karnik, R.; Fan, R.; Yue, M.; Li, D. Y.; Yang, P. D.; Majumdar, A. *Nano Lett.* **2005**, *5*, 943–948.
(15) Diakova, G.; Goddard, Y. A.; Korb, J. P.; Bryant, R. G. *J. Magn. Reson.* **2007**, *189*, 166–172.
(16) Pal, S. K.; Peon, J.; Bagchi, B.; Zewail, A. H. *J. Phys. Chem. B* **2002**, *106*, 12376–12395.
(17) Pal, S. K.; Zewail, A. H. *Chem. Rev.* **2004**, *104*, 2099–2123.

(18) Upadhyayula, V. K. K.; Deng, S.; Mitchell, M. C.; Smith, G. B. *Sci. Total Environ.* **2009**, *408*, 1−13.
(19) Lu, C.; Chung, Y. L.; Chang, K. F. *Water Res.* **2005**, *39*, 1183−1189.
(20) Zhou, Q.; Xiao, J.; Wang, W.; Liu, G.; Shi, Q.; Wang, J. *Talanta* **2006**, *68*, 1309−1315.
(21) Kandah, M. I.; Meunier, J. L. *J. Hazard. Mater.* **2007**, *146*, 283−288.
(22) Maniwa, Y.; Kataura, H.; Abe, M.; Udaka, A.; Suzuki, S.; Achiba, Y.; Kira, H.; Matsuda, K.; Kadowaki, H.; Okabe, Y. *Chem. Phys. Lett.* **2005**, *401*, 534−538.
(23) Koga, K.; Gao, G. T.; Tanaka, H.; Zeng, X. C. *Phys. A (Amsterdam, Neth.)* **2002**, *314*, 462−469.
(24) Kolesnikov, A. I.; Loong, C. K.; Souza, N. R. d.; Burnham, C. J.; Moravsky, A. P. *Phys. B (Amsterdam, Neth.)* **2006**, *385*−*386*, 272−274.
(25) Kolesnikov, A. I.; Zanotti, J. M.; Loong, C. K.; Thiyagarajan, P.; Moravsky, A. P.; Loutfy, R. O.; Burnham, C. J. *Phys. Rev. Lett.* **2004**, *93*, 035503.
(26) Guillot, B. *J. Mol. Liq.* **2002**, *101*, 219−260.
(27) Lynden-Bell, R. M.; Rasaiah, J. C. *J. Chem. Phys.* **1996**, *105*, 9266−9280.
(28) Hummer, G.; Rasaiah, J. C.; Noworyta, J. P. *Nature* **2001**, *414*, 188−190.
(29) Striolo, A.; Chialvo, A. A.; Gubbins, K. E.; Cummings, P. T. *J. Chem. Phys.* **2005**, *122*, 234712.
(30) Striolo, A.; Gubbins, K. E.; Chialvo, A. A.; Cummings, P. T. *Adsorption* **2005**, *11*, 337−341.
(31) Striolo, A.; Gubbins, K. E.; Gruszkiewicz, M. S.; Cole, D. R.; Simonson, J. M.; Chialvo, A. A. *Langmuir* **2005**, *21*, 9457−9467.
(32) Striolo, A.; Naicker, P. K.; Chialvo, A. A.; Cummings, P. T.; Gubbins, K. E. *Adsorption* **2005**, *11*, 397−401.
(33) Lakatos, G.; Patey, G. N. *J. Chem. Phys.* **2007**, *126*, 024703.
(34) Srivastava, R.; Docherty, H.; Singh, J. K.; Cummings, P. T. *J. Phys. Chem. C* **2011**, *115*, 12448−12457.
(35) Gordillo, M. C.; Marti, J. *Chem. Phys. Lett.* **2000**, *329*, 341−345.
(36) Gordillo, M. C.; Marti, J. *Chem. Phys. Lett.* **2001**, *341*, 250−254.
(37) Kyakuno, H.; Matsuda, K.; Yahiro, H.; Inami, Y.; Fukuoka, T.; Miyata, Y.; Yanagi, K.; Maniwa, Y.; Kataura, H.; Saito, T.; Yumura, M.; Iijima, S. *J. Chem. Phys.* **2011**, *134*244501.
(38) Kolafa, J.; Nezbeda, I. *Fluid Phase Equilib.* **1994**, *100*, 1−34.
(39) Kumari, M.; Dass, N. *J. Phys.: Condens. Matter* **1990**, *2*, 3219−3229.
(40) Holzapfel, W. B. *Phys. Rev. B* **2003**, *67*, 026102.
(41) Parsafar, G.; Farzi, N.; Najafi, B. *Int. J. Thermophys.* **1997**, *18*, 1197−1216.
(42) Parsafar, G.; Mason, E. A. *Phys. Rev. B* **1994**, *49*, 3049−3060.
(43) Parsafar, G.; Mason, E. A. *J. Phys. Chem.* **1994**, *98*, 1962−1967.
(44) Parsafar, G.; Mason, E. A. *J. Phys. Chem.* **1993**, *97*, 9048−9053.
(45) Parsafar, G. A.; Spohr, H. V.; Patey, G. N. *J. Phys. Chem. B* **2009**, *113*, 11977−11987.
(46) Nasrifar, K.; Jalali, F. *Fluid Phase Equilib.* **2003**, *207*, 167−181.
(47) Parsafar, G. A.; Kermanpour, F.; Najafi, B. *J. Phys. Chem. B* **1999**, *103*, 7287−7292.
(48) Berendsen, H. J. C.; Grigera, J. R.; Straatsma, T. P. *J. Phys. Chem.* **1987**, *91*, 6269−6271.
(49) Tjatjopoulos, G. J.; Feke, D. L., Jr.; J. A. M.. *J. Phys. Chem.* **1988**, *92*, 4006−4007.
(50) Allen, M. P.; Tildesley, D. J. *Computer Simulation of Liquids*; Clarendon Press: Oxford, 1991.
(51) Frenkel, D.; Smit, B. *Understanding Molecular Simulation: From Algorithms to Applications*: Academic Press: London, 2002.
(52) Mikami, F.; Matsuda, K.; Kataura, H.; Maniwa, Y. *ACS Nano* **2009**, *3*, 1279−1287.
(53) Metropolis, N.; Rosenbluth, A. W.; Rosenbluth, M. N.; Teller, A. H. *J. Chem. Phys.* **1953**, *21*, 1087−1092.